2.G

Nuclear Physics **A230** (1974) 317—328; © *North-Holland Publishing Co., Amsterdam*

INVESTIGATION OF THE ^{26}Mg(d, p)^{27}Mg REACTION

F. MEURDERS and A. VAN DER STELD

Fysisch Laboratorium, Rijksuniversiteit, Utrecht, The Netherlands

Received 13 June 1974

Abstract: The angular distributions of 31 protons groups from the ^{26}Mg(d, p)^{27}Mg reaction have been measured at $E_d = 12.0$ MeV with a split-pole magnetic spectrograph. Excitation energies have been determined for 29 bound states. Three new levels have been found. A DWBA analysis yields l_n values for 19 levels; two different least-squares procedures are discussed for this purpose. The deduced spectroscopic factors are compared with various shell model calculations.

E NUCLEAR REACTION ^{26}Mg(d, p), $E = 12.0$ MeV; measured $\sigma(E_p, \theta)$.
^{27}Mg deduced levels, l_n and S; enriched target.

1. Introduction

Recently, several experiments have been performed to obtain information on the electromagnetic properties of ^{27}Mg levels. Branching and mixing ratios were determined [1-5]. The ^{26}Mg(d, p)^{27}Mg reaction has been investigated only summarily. Proton spectra have been taken either at low energy resolution ($\approx$ 100 keV) [refs. [6, 7])], or at 20 keV resolution but at only four angles [8]). Consequently it was thought worthwhile to investigate this reaction in more detail to obtain reliable experimental spectroscopic factors which can be compared with shell model calculations. In the present experiment the ^{26}Mg(d, p)^{27}Mg reaction ($Q = 4.22$ MeV) was studied at $E_d = 12.0$ MeV with a magnetic spectrograph.

2. Experiment

Deuterons were accelerated to 12.0 MeV with the 6 MV tandem Van de Graaff generator of the Utrecht University. The protons produced were detected with seven position sensitive detectors placed in the focal plane of an Enge split-pole spectrograph. Deuterons and α-particles were absorbed by teflon foils in front of the detectors. Energy straggling in foils and detectors was eliminated by dividing the detector position signals by their corresponding energy signals with a CDC 1700 on-line computer system [9]).

The targets consisted of 20 to 50 μg/cm^2 99.4 % enriched ^{26}Mg evaporated onto 20 μg/cm^2 carbon foils.

Three different settings of the detectors were necessary to cover the whole spectrum up to 6 MeV excitation energy. Angular distributions were measured between $\theta = 5°$

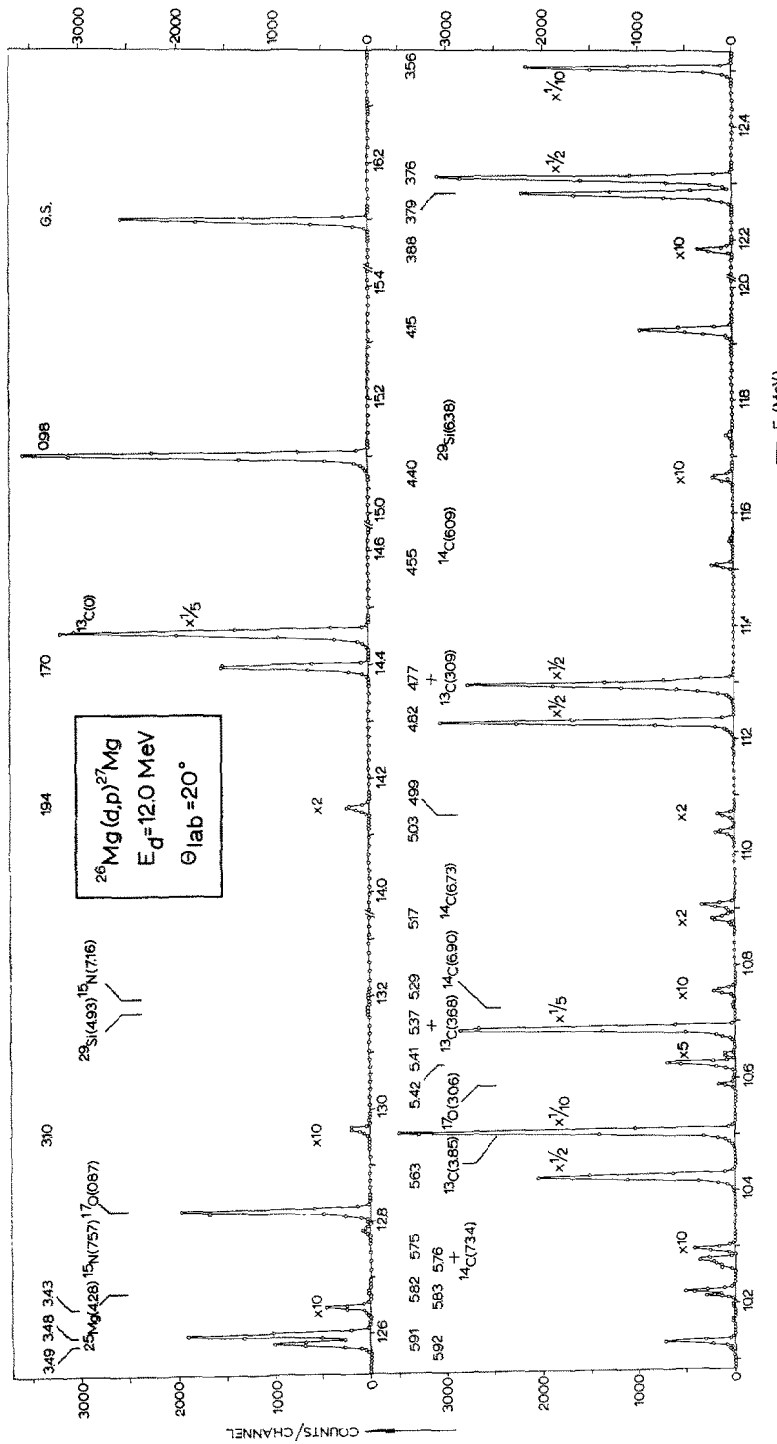

Fig. 1. Proton groups from the ^{26}Mg(d, p)^{27}Mg reaction measured at $\theta = 20°$. The ^{27}Mg peaks are labeled with the excitation energies of the corresponding levels. The contaminant groups are indicated by final nucleus and excitation energy.

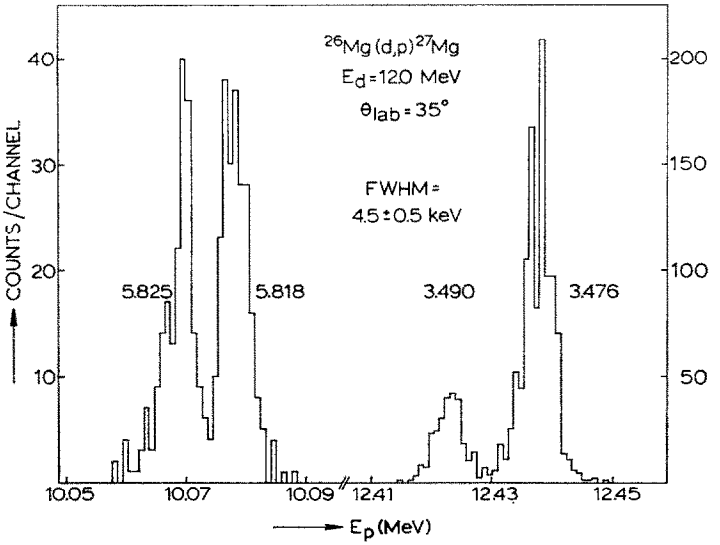

Fig. 2. High-resolution measurement of the 3.48-3.49 MeV and 5.82-5.83 MeV doublets with a 1.5 cm position sensitive detector.

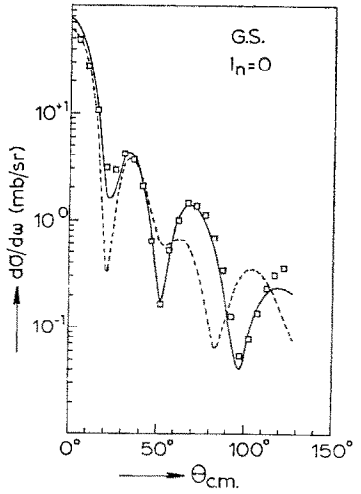

Fig. 3. The DWBA fits to the experimental angular distribution of the ground-state transition with deuteron parameters from ref. [15]) (dotted line) and the deuteron parameters from table 1, column [a]) (full line).

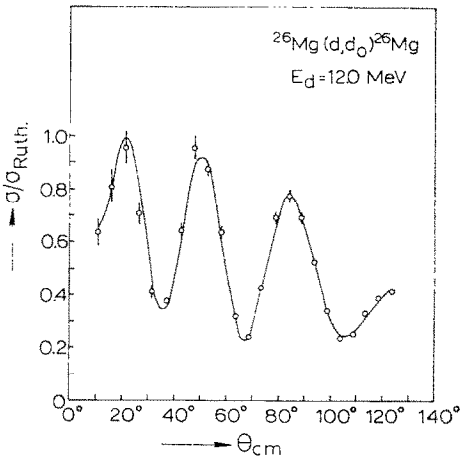

Fig. 4. Angular distribution of the deuterons from the ^{26}Mg(d, d_0) reaction at $E_d = 12.0$ MeV. The full curve is calculated with the parameters of table 1, column [a]).

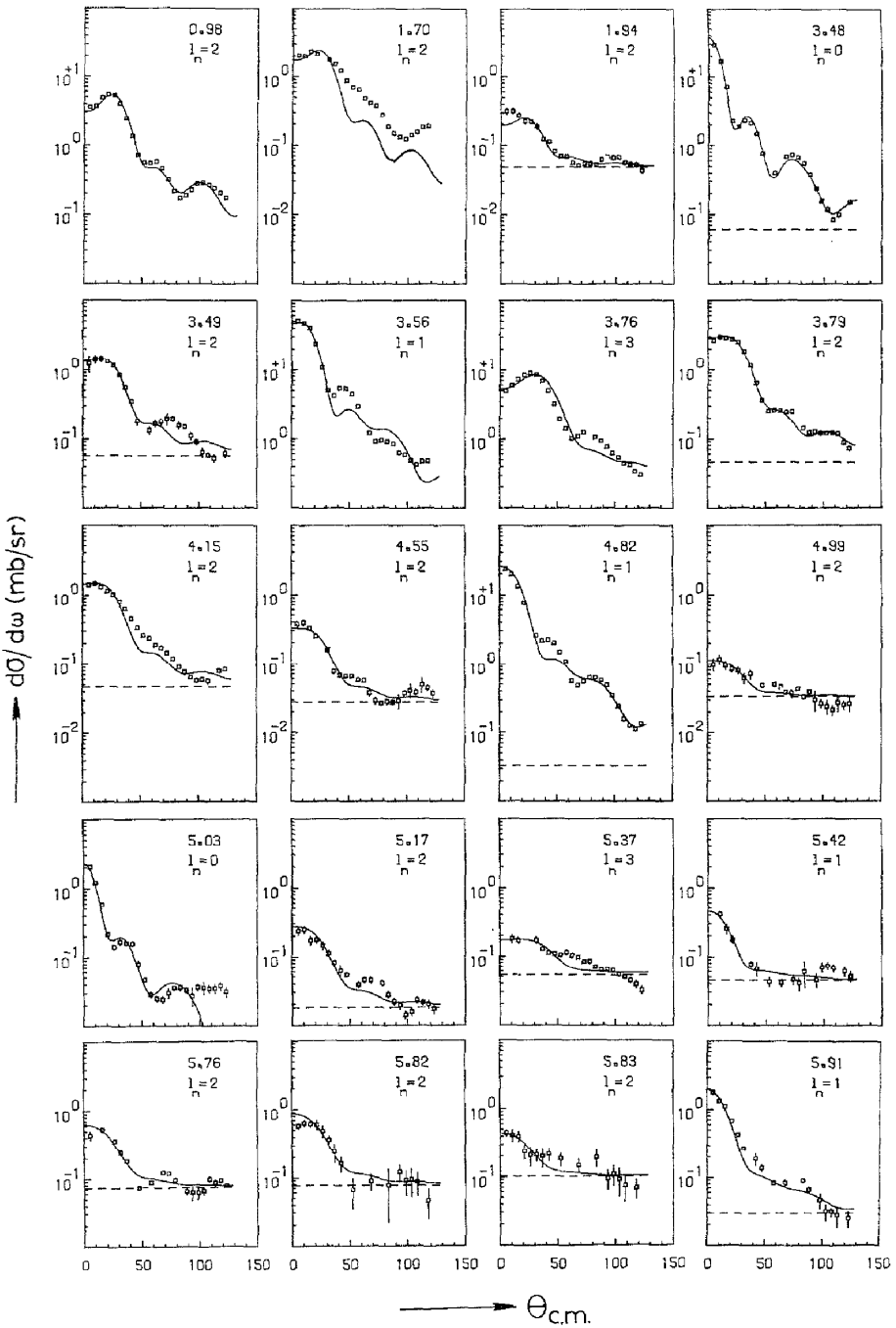

Fig. 5. Experimental $^{26}Mg(d, p)^{27}Mg$ differential cross sections. The full line gives the total calculated cross section which is the sum of the DWBA contribution and the compound nucleus contribution (horizontal dotted line). Only the levels which show a stripping pattern are displayed.

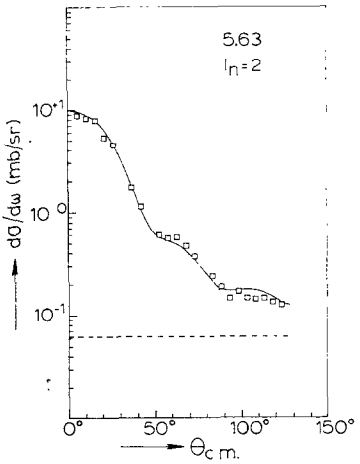

Fig. 6. Experimental angular distribution for the 5.63 MeV level in the ^{26}Mg(d, p) reaction. The full line gives the total calculated cross section which is the sum of the DWBA contribution and the compound nucleus contribution (horizontal dotted line).

and 120° in steps of 5°. The numbers of counts were normalized to the number of elastically scattered deuterons, detected with a Si detector in the target chamber. For each setting of the detectors the angular distribution of the first excited state was measured as an additional check.

TABLE 1

Optical model parameters

	Deuteron		Proton		Neutron
	[a]	[b]	[c]	[d]	[e]
V_0 (MeV)	95.2	104.1	$58.3-0.32\,E_p$	$57.9-0.55\,E_p$	[g]
a_0 (fm)	0.836	0.85	0.75	0.65	0.65
r_0 (fm)	1.0485	1.05	1.17	1.25	1.25
W_V (MeV)			$0.22\,E_p-2.7$ [f]		
W_d (MeV)	24.14	10.12	$13.13-0.25\,E_p$	9.0	
a_W (fm)	0.619	0.56	0.59	0.47	
r_W (fm)	1.399	1.63	1.32	1.25	
V_s (MeV)	7.0	7.0	6.2	7.5	$\lambda_{s,o.} = 25$
a_s (fm)	0.6	0.6	0.75	0.65	0.65
r_s (fm)	0.9	0.9	1.01	1.25	1.25
r_c (fm)	1.3	1.3	1.36	1.25	

[a]) Present experiment.
[b]) Ref. [15]).
[c]) Ref. [14]).
[d]) Ref. [13]).
[e]) Ref. [16]).
[f]) Only for $W_V > 0$.
[g]) Fitted to the binding energy.

TABLE 2

Spectroscopic data

Literature [a])		Present experiment				Shell model calculations		
E_x (keV)	J^π	E_x (d, p) (keV)	l_n	$(2J+1)S_n$		$(2J+1)S_n$		
				$J = l_n - \frac{1}{2}$	$J = l_n + \frac{1}{2}$	[b])	[c])	[d])
0	$\frac{1}{2}^+$		0		1.5	1.4	0.85	1.2
984.6 ± 0.2	$\frac{3}{2}^+$		2	2.4		1.6	1.1	
1698.3 ± 0.2	$\frac{5}{2}^+$	1699 ± 6	2		0.76	0.15	0.11	0.53
1939.9 ± 0.3	$\frac{5}{2}^+$	1939 ± 8	2		0.057	0.07	0.12	0.17
3109.1 ± 0.5	$(\frac{3}{2}^+, \frac{7}{2}^+)$	3104 ± 5						
3427 ± 10		3426 ± 5						
3476.1 ± 0.5	$\frac{1}{2}^+$	3479 ± 6	0		0.58	0.22	0.074	0.018
3485 ± 3	$(\frac{3}{2}, \frac{5}{2})^+$	3490 ± 2	2	0.28	0.24	1.0 [e])	0.69 [e])	
3560.6 ± 0.8	$\frac{3}{2}^-$	3559 ± 6	1		1.6			
3761.8 ± 0.4	$\frac{7}{2}^-$	3763 ± 8	3		4.5			
3786.2 ± 1.4	$\frac{3}{2}^+$	3786 ± 8	2	0.58		0.52	0.33	
3884 ± 10	$> \frac{1}{2}$							
4154 ± 10	$(\frac{3}{2}, \frac{5}{2})^+$	4150 ± 6	2	0.23	0.20	0.06 [f])	0.001 [f])	
4391 ± 3		4399 ± 8						
4544 ± 3	$(\frac{3}{2}^+, \frac{5}{2}^+)$	4553 ± 6	2	0.040	0.034	0.08 [e])	0.03 [e])	
4771 ± 10		4770 ± 8						
4824 ± 4	$(\frac{1}{2}^-, \frac{3}{2}^-)$	4824 ± 8	1	0.64	0.62			
4986 ± 10		4991 ± 6	(2)	(0.008)	(0.007)			
5020 ± 10		5025 ± 6	0		0.048	0.02	0.003	0.002
(5169 ± 15)		5170 ± 5	2	0.026	0.022			
5292 ± 15		5294 ± 5						
5365 ± 15		5367 ± 5	(3)	(0.054)	(0.040)			
5405 ± 15		5407 ± 6						
		5419 ± 6	1	0.009	0.008			
5618 ± 15		5625 ± 5	2	0.79	0.68			
5742 ± 15		5745 ± 5						
5762 ± 15		5763 ± 5	2	0.043	0.037			
		5818 ± 7	2	0.062	0.053			
5817 ± 15		5825 ± 7	(2)	(0.027)	(0.023)			
5922 ± 15		5906 ± 7	1	0.046	0.046			
		5919 ± 7						

[a]) Ref. [12]).

[b]) Calculations in a truncated $1d_{\frac{5}{2}}2s_{\frac{1}{2}}1d_{\frac{3}{2}}$ configuration space [23]).

[c]) The ^{26}Mg ground state in a $1d_{\frac{5}{2}}2s_{\frac{1}{2}}$ configuration space coupled with a $1d_{\frac{5}{2}}2s_{\frac{1}{2}}1d_{\frac{3}{2}}$ configuration space for ^{27}Mg.

[d]) Calculations in a $1d_{\frac{5}{2}}2s_{\frac{1}{2}}$ configuration space [21]).

[e]) Calculated for $J = \frac{3}{2}$.

[f]) Calculated for $J = \frac{5}{2}$.

Fig. 1 shows the proton spectrum at 20°. The average background is less than 2 counts per channel, whereas the strongest peak, corresponding to the 3.56 MeV level of ^{27}Mg, rises to about 2×10^4 counts per channel. Due to contaminants in the targets, levels of ^{13}C, ^{14}C, ^{15}N, ^{17}O, ^{25}Mg and ^{29}Si were also excited. The average resolution is 7 keV (FWHM). Peaks corresponding to levels of ^{13}C, ^{14}C, ^{15}N and ^{17}O, of which the energies and Q-values are accurately known [10, 11]), have been

used to determine excitation energies in ^{27}Mg. The resulting errors range from 5 to 8 keV (see, table 2). Systematic errors, due to an inhomogeneous distribution of the contaminants in the target, are negligible because the targets used were quite thin. No good determination of the excitation energy was possible for the $E_x = 0.98$ and 3.88 MeV levels. A special effort has been directed towards separating the members of three hitherto unknown doublets at 5.42, 5.82 and 5.91 MeV. For this purpose a 1.5 cm long detector with high position resolution has been used. The resolution in this run was 4.5 keV (FWHM) and the separation of the doublet members was found as 12 ± 2, 7 ± 2 and 13 ± 3 keV, respectively. The narrowest doublet at 5.82 MeV is show in fig. 2, where also the already known doublet at 3.48 MeV is given. For the latter doublet a separation was found of 14 ± 2 keV. The weak component has not been seen in previous (d, pγ) experiments [2, 3, 5]. The excitation energy has only been determined from (n, γ) work as 3485 ± 3 keV [ref. [4])]. The excitation energy of the strong component is accurately known as 3476.1 ± 0.5 keV [ref. [12])] from which the excitation energy of the weak component could now be determined as 3490 ± 2 keV (table 2).

Absolute cross sections were found by comparing at forward angles the yield of elastic deuteron scattering and ^{26}Mg(d, p)^{27}Mg, $E_x = 0.98$ MeV at $E_d = 12.0$ MeV. The elastic cross section was determined in two ways:

(i) By measuring Rutherford scattering at 3 MeV and elastic scattering at 12 MeV with the same target and with detectors placed at forward angles in a 60 cm diam. scattering chamber.

(ii) By an optical model fit to the 12 MeV elastic scattering data with the use of the parameters from table 1, set a (see fig. 4 and sect. 3). The results of methods (i) and (ii) differ by about 4 %.

The angular distributions of all proton groups are displayed in figs. 3, 5 and 6 where only statistical errors are indicated.

3. Analysis

To analyse the measured angular distributions, theoretical curves were calculated with the DWBA code DWUCK. The Perey [13]) and the Becchetti and Greenlees [14]) overall parameters were used for the proton optical potential. The shape of the calculated distributions turns out to be almost identical for the two parameter sets. However, the Becchetti-Greenlees absolute cross section is smaller than the Perey one by 15, 17, 20 and 25 % for $l_n = 0$, 1, 2 and 3 transitions, respectively. Similar results were found in ref. [34]). Because of somewhat better agreement with the experimental angular distributions the Becchetti-Greenlees proton parameters were chosen.

An overall deuteron optical model potential is given by Schwandt and Haeberli [ref. [15])]. However, their parameters give a poor fit to the angular distributions as is illustrated in fig. 3 for the ground-state group. Therefore, the 12 MeV deuteron

elastic scattering angular distribution was measured. The data were taken in the range $\theta = 10°$–$120°$ in steps of 5°, see fig. 4. With the Schwandt-Haeberli parameters as start values a best-fit set has been found with the optical model search code of Perey, see table 1. Only the imaginary part is quite different from the Schwandt-Haeberli potential. Fig. 4 shows the result of the optical model fit with the best parameter set. It has been calculated without a spin-orbit coupling term which neglect hardly influences the result.

The range and diffuseness parameters for the neutron potential were taken as 1.25 and 0.65 fm, respectively, see table 1. The calculations were carried out with a non-locality parameter of 0.54 fm for the deuterons and 0.85 fm for the protons [ref. [16])]. The finite-range parameter for the neutron-proton interaction was taken as 0.621 fm. No radial cut-off has been used.

Since the target spin is zero, the spectroscopic factor S_n is deduced from $\sigma_{exp}(\theta) = 1.53(2J_f+1)S_n\sigma_{DWBA}(\theta)$, where J_f is the spin of the final state, $\sigma_{exp}(\theta)$ the experimental cross section and $\sigma_{DWBA}(\theta)$ the DWBA cross section.

In figs. 5 and 6 all measured angular distributions which show a stripping pattern are given. The levels, for which the angular distributions show no stripping pattern, are mainly excited through compound nucleus formation. The differential cross section for these levels is almost independent of angle and of the order of 50 μb/sr. Therefore we have assumed that weak compound contributions can be taken constant as a function of angle. For levels which show a stripping character a least-squares program has been used to perform a simultaneous fit of a constant compound reaction cross section and a direct reaction cross section. The compound nucleus contribution has been neglected whenever it did not improve the fit. Only fitted compound nucleus contributions of the order of 50 μb/sr are considered to be realistic and are taken into account. The l_n value is mainly determined by the position of the first maximum and the steepness of the following slope. The spectroscopic factor is also mainly determined by the cross section at forward angles. Due to the earlier stated uncertainties in the proton optical potential parameters and to uncertainties in the deuteron parameters, a systematic error of 25 % has been assigned to the spectroscopic factors obtained [17]). For weakly excited states the relatively large compound nucleus contribution may lead to even larger errors.

4. Results

To 19 levels an unambiguous l_n value could be assigned (see table 2). None of these conflict with known spins and parities. The deduced spectroscopic factors are also given in table 2.

Most of the angular distributions are rather well reproduced by the DWBA calculations. A remarkable deviation is found for the 1.70 MeV state which is known to have $J^\pi = \frac{5}{2}^+$. Other strong $l_n = 2$ groups which lead to states with known $J^\pi = \frac{3}{2}^+$ ($E_x = 0.98$ and 3.79 MeV), however, turn out to be well fitted by DWBA.

Clearly, DWBA is not able to account for this spin dependence. Possibly, coupled-channels calculations will do better [18, 19]). So far the shape of the observed distributions is only an indication for the spin. The shape of the strong $l_n = 2$ groups suggests $J^\pi = \frac{3}{2}^+$ for levels at $E_x = 3.49$, 4.55, 5.17 and 5.63 MeV, and $J^\pi = \frac{5}{2}^+$ for the 4.15 MeV level. The angular distribution of the high-lying 5.63 MeV level is very well reproduced by the DWBA curve (see fig. 6). The transition to the 4.82 MeV level is unambiguously determined as $l_n = 1$, so that this level has negative parity. This is in contrast with the $l_n = 0$ result (obtained at $E_d = 3.1$ MeV) of ref. [20]). The known difference at backward angles between transitions to $\frac{1}{2}^-$ and $\frac{3}{2}^-$ states suggests $J = \frac{1}{2}$ for the 4.82 MeV level. Other experiments will be needed to determine these suggested spin values uniquely.

5. Least-squares procedures

It would be attractive to have an objective quantitative criterion to assign unique l_n values to measured angular distributions. A criterion that replaces the qualitative arbitrariness of the more or less experienced human eye.

Once a criterion has been formulated, it can be tested on transitions with unambiguously known l_n values. It may be hoped that in a latter stage such a criterion may be of some help in assigning l_n values to weaker transitions, like those to the 4.99, 5.37 and 5.83 MeV levels in the present work.

A commonly used procedure in a quantitative comparison of experiment and theory is the minimization of the quantity Q^2, which gives the squared deviation between theory and experiment, weighted by the experimental error. However, since DWBA does not reproduce the exact angular distribution, but is at best a good approximation, a χ^2 probability distribution cannot be used. The Q^2 value then increases with increasing experimental accuracy. For all the low-lying levels the l_n assignment on the basis of the Q^2 value is in agreement with the already known values, except for the 1.70 MeV $J^\pi = \frac{5}{2}^+$ level. The Q^2 values for this level and for the $l_n = 0$, 1, 2 and 3 transfer corresponding to $E_x = 3.48$, 3.56, 3.49 and 3.76 MeV, respectively, are listed in table 3. In order to avoid difficulties from the unknown compound nucleus cross section, the Q^2 value is calculated for $\theta \leqq 60°$.

If the experimental errors are small compared to the uncertainty in the theory, the quantity $K^2 = \sum_{\theta \leqq 60°} [(\sigma_{exp}(\theta) - \sigma_{DWBA}(\theta))/\sigma_{exp}(\theta)]^2$ can profitably be used for a direct comparison of theory and experiment. The value of K^2 depends on the transferred orbital momentum. In fig. 7 a K^2 histogram is plotted for $d_{\frac{5}{2}}$ and $d_{\frac{3}{2}}$ neutron transfer in the sd shell at deuteron energies between 7 and 21 MeV. Only those transitions have been taken into account where the target spin and final spin yield a unique $l_n = 2$ and transferred spin value. Weakly excited levels were ignored. The fact that the mean K^2 value in fig. 7. for the $d_{\frac{5}{2}}$ transitions is considerably larger than the $d_{\frac{3}{2}}$ value demonstrates the failure of DWBA to reproduce the difference between the experimental angular distributions for $d_{\frac{5}{2}}$ and $d_{\frac{3}{2}}$ neutron transfer. The theoretical

TABLE 3

Least-squared values for the ^{26}Mg(d, p)^{27}Mg reaction

E_x (MeV)	J^π	l_n	J_s [a]	K^2 [b]				Q^2 [c]			
				$l_n = 0$	1	2	3	$l_n = 0$	1	2	3
1.70	$\frac{5}{2}^+$	2		9	7	3	1.1	600	510	170	50
3.48	$\frac{1}{2}^+$	0		0.3	4	3	3	15	360	320	300
3.49	$(\frac{3}{2}, \frac{5}{2})^+$	2	$\frac{3}{2}$	13	4	0.2	4	60	40	1.8	30
3.56	$\frac{3}{2}^-$	1		4	1.0	4	4	760	190	690	710
3.76	$\frac{7}{2}^-$	3		9	6	3	0.4	500	370	170	20
4.15	$(\frac{3}{2}, \frac{5}{2})^+$	2	$\frac{5}{2}$	7	4	1.3	1.8	290	170	50	60

[a]) Suggested J-value.

[b]) $K^2 = \Sigma_{\theta \leqq 60°}[(\sigma_{th}(\theta) - \sigma_{exp}(\theta))/\sigma_{exp}(\theta)]^2$, normalised at 12 angles.

[c]) $Q^2 = N^{-1}\Sigma_{\theta \leqq 60°}[(\sigma_{th}(\theta) - \sigma_{exp}(\theta))/\Delta\sigma_{exp}(\theta)]^2$, where N is the number of experimental points minus the number of fitted parameters.

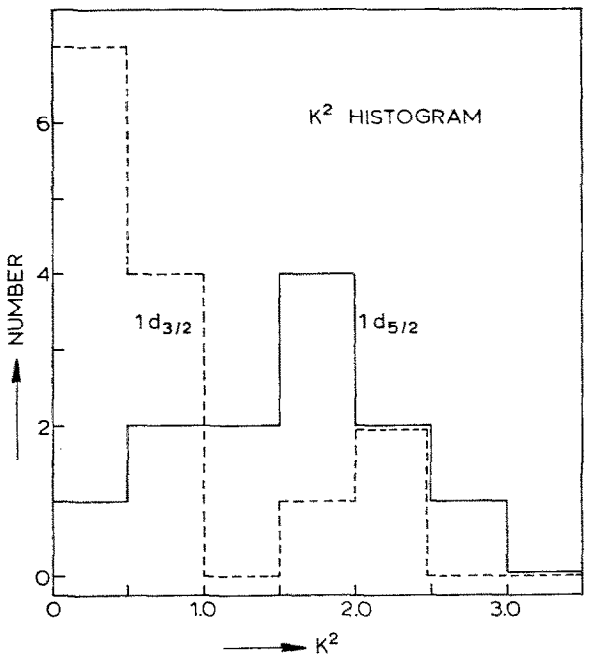

Fig. 7. Histogram of K^2 values for $d_{\frac{3}{2}}$ and $d_{\frac{5}{2}}$ neutron transfer in (d, p) reactions in the sd shell at deuteron energies between 7 and 21 MeV. The values are calculated from (d, p) reactions leading to ^{21}Ne, ^{22}Ne, ^{23}Ne, ^{24}Na, ^{26}Mg, ^{29}Si, ^{31}Si, ^{32}P, ^{33}S, ^{34}S, ^{35}S, ^{37}Ar and ^{41}Ca [refs. [27-36])]. Also the present results are included.

description for the $d_{\frac{3}{2}}$ angular distribution is much better than for $d_{\frac{5}{2}}$. The broad range of K^2 values in fig. 7 shows the differences in the goodness of the various fits as a result of the optical model potentials used.

Table 3 shows that for the ^{26}Mg(d, p)^{27}Mg reaction, both Q^2 and K^2 properly differentiate between $l_n = 0$, $l_n = 1$, $1d_{\frac{3}{2}}$ and $l_n = 3$ transfer. This is of course due to

the outspoken differences in both slope and width of the first stripping maxima. For $1d_{\frac{5}{2}}$ and $l_n = 3$ transfer, however, K^2 and Q^2 do not differentiate sufficiently. For the $l_n = 2$, $J^\pi = \frac{5}{2}^+$ level at 1.70 MeV both quantities have a lower value for $l_n = 3$ than for $l_n = 2$. This failure is due to the flatness of the experimental $d_{\frac{5}{2}}$ angular distribution between 20° and 50°. Around $E_d = 12$ MeV, moreover, the width of the main $1d_{\frac{5}{2}}$ stripping maximum is very similar to that of an $l_n = 3$ distribution. The two features together result in a poor distinction between $1d_{\frac{5}{2}}$ and $l_n = 3$ transfer. This is also shown for the 4.15 MeV level (see table 3), which has a suggested J-value of $\frac{5}{2}$ (see above). For this level K^2 and Q^2 have lower values for $l_n = 2$. The K^2 method is somewhat more sensitive than the Q^2 criterion in this case. For a reliable distinction between $1d_{\frac{5}{2}}$ and $l_n = 3$ transfer a better theoretical description is certainly needed. For the other cases, and also for the weakly excited levels, the l_n assignment on the basis of the lowest K^2 and Q^2 value is in agreement with the result of the experienced human eye, provided that the next best value is higher by at least a factor of 2.

6. Comparison with shell model calculations

If one describes the target nucleus ^{26}Mg by a simple $(\pi d_{\frac{5}{2}})^{-2}$ configuration, then the lowest states in ^{27}Mg are expected to show a strong single-particle character, as either an $s_{\frac{1}{2}}$ or a $d_{\frac{3}{2}}$ neutron is added. This is indeed found experimentally (see table 2). Also, the (suggested) $d_{\frac{3}{2}}$ transition to the 5.63 MeV level is remarkably strong, as fig. 6 shows. However, neutron stripping to $\frac{5}{2}^+$ states is not allowed since in this simple shell model picture the $d_{\frac{5}{2}}$ neutron orbit is filled. This reasonably agrees with experiment where very small spectroscopic factors are found for known $J^\pi = \frac{5}{2}^+$ states, except perhaps for the lowest one at $E_x = 1.70$ MeV (see table 2). The spectroscopic factors for the lowest two negative parity states, at 3.56 MeV ($J^\pi = \frac{3}{2}^-$) and 3.76 MeV ($J^\pi = \frac{7}{2}^-$) are rather large such that important components in the wave functions of the states may be $d_{\frac{5}{2}}^{-2}p_{\frac{3}{2}}$ and $d_{\frac{5}{2}}^{-2}f_{\frac{7}{2}}$, respectively.

For positive parity states more detailed shell model calculations exist such that a comparison can be made between different shell model results for the spectroscopic factors and the experimental values. In ref. [21]) the calculations were carried out in a complete $1d_{\frac{5}{2}}2s_{\frac{1}{2}}$ configuration space with ^{16}O as an inert core. The two-body matrix elements as well as the single-particle energies were found empirically. The calculated spectroscopic factors for the ground state and the first $\frac{5}{2}^+$ state agree reasonably well with the experimental values, as is shown in table 2, column d.

We have computed the spectroscopic factors of the lowest $\frac{1}{2}^+$ and $\frac{5}{2}^+$ states as well as of the $\frac{3}{2}^+$ states, by using wave functions for ^{27}Mg levels in a truncated $1d_{\frac{5}{2}}2s_{\frac{1}{2}}1d_{\frac{3}{2}}$ configuration space [22]) and the wave function of the ^{26}Mg ground state in the $1d_{\frac{5}{2}}2s_{\frac{1}{2}}$ configuration [21]). Only those configurations have been taken into account which contribute at least 1 % in intensity. In order to compare the theoretical values with the experimental results, the spins suggested by the J-dependence of the angular distributions were assumed to be correct for the 3.49, 4.15 and 4.55 MeV levels. The

agreement with experiment is not too bad (see table 2, column c), although the $1d_{\frac{3}{2}}$ subshell is neglected in the ^{26}Mg ground state.

Very recently, calculations have been performed in which the configuration space for ^{26}Mg has been extended to include the $1d_{\frac{3}{2}}$ subshell [23]). The ^{27}Mg wave functions are again those of ref. [22]). A maximum of four holes was allowed in the $1d_{\frac{5}{2}}$ subshell and a modified surface delta interaction (MSDI) was used as Hamiltonian [24, 25]). The results for the ground state and some excited states are in excellent agreement with the experimental values (see table 2, column b). For other states the agreement is rather poor. For example, the sum of the calculated spectroscopic strengths [26]) for the $\frac{5}{2}^+$ states (0.28) is about four times smaller than the experimental value (1.04) so that this model underestimates the number of $d_{\frac{5}{2}}$ neutron holes in the ^{26}Mg ground state.

References

1) J. M. Lacambra, D. R. Tilley and N. R. Roberson, Nucl. Phys. **A92** (1967) 30
2) D. H. Sykes *et al.*, Nucl. Phys. **A135** (1969) 335
3) G. Costa and F. A. Beck, Nucl. Phys. **A181** (1972) 132
4) E. Selin and E. Wallander, Nucl. Phys. **A150** (1970) 305
5) B. Skaali, Phys. Norv. **4** (1969) 45
6) J. Silverstein, L. J. Lidofsky, G. E. Mitchell and R. B. Weinberg, Phys. Rev. **136** (1964) B1703
7) R. N. Glover, Phys. Lett. **16** (1965) 147
8) B. Cujec, Phys. Rev. **136** (1964) B1305
9) P. B. J. van Elswijk, R. Engmann, A. M. Hoogenboom and P. de Wit, Nucl. Instr. **96** (1971) 35
10) F. Ajzenberg-Selove, Nucl. Phys. **A152** (1970) 1
11) F. Ajzenberg-Selove, Nucl. Phys. **A166** (1971) 1
12) P. M. Endt and C. van der Leun, Nucl. Phys. **A214** (1973) 1
13) F. G. Perey, Phys. Rev. **131** (1963) 745
14) F. D. Becchetti and G. W. Greenlees, Phys. Rev. **182** (1969) 1190
15) P. Schwandt and W. Haeberli, Nucl. Phys. **A123** (1969) 401
16) K. K. Seth, J. Picard and G. R. Satchler, Nucl. Phys. **A140** (1970) 577
17) L. L. Lee *et al.*, Phys. Rev. **136** (1964) B971
18) U. Scheib, A. Hofmann, G. Philipp and F. Vogler, Nucl. Phys. **A203** (1973) 177
19) R. Mackintosh, Nucl. Phys. **A170** (1971) 353
20) S. Koh and Y. Oda, Phys. Rev. **C4** (1973) 2501
21) B. H. Wildenthal, J. B. McGrory, E. C. Halbert and P. W. M. Glaudemans, Phys. Lett. **26B** (1968) 692 and private communication
22) B. H. Wildenthal and J. B. McGrory, Phys. Rev. **C7** (1973) 714 and private communication
23) M. J. A. de Voigt and B. H. Wildenthal, Nucl. Phys. **A206** (1973) 305
24) P. W. M. Glaudemans, B. H. Wildenthal and J. B. McGrory, Phys. Lett. **21** (1966) 427
25) P. W. M. Glaudemans, P. J. Brussaard and B. H. Wildenthal, Nucl. Phys. **A102** (1967) 593
26) J. B. French and M. H. Macfarlane, Nucl. Phys. **26** (1961) 168
27) A. J. Howard, J. G. Pronko and C. A. Whitten, Nucl. Phys. **A152** (1970) 317
28) P. Neogy, R. Middleton and W. Scholz, Phys. Rev. **C6** (1972) 885
29) C. Daum, Nucl. Phys. **45** (1963) 273
30) H. F. Lutz and S. F. Eccles, Nucl. Phys. **88** (1966) 513
31) M. C. Mermaz *et al.*, Phys. Rev. **C4** (1971) 1778
32) B. H. Wildenthal and P. W. M. Glaudemans, Nucl. Phys. **A108** (1968) 49
33) J. J. M. van Gasteren, A. J. L. Verhage and J. F. van der Veen, Nucl. Phys. **A210** (1973) 29
34) J. G. van der Baan and B. R. Sikora, Nucl. Phys. **A173** (1971) 456
35) J. G. van der Baan and H. G. Leighton, Nucl. Phys. **A170** (1971) 607
36) T. A. Belote, A. Sperduto and W. W. Buechner, Phys. Rev. **139** (1965) B80